JOC The Journal of Organic Chemistry

Article

pubs.acs.org/joc

On the Origin of Regio- and Stereoselectivity in Singlet Oxygen Addition to Enecarbamates

Ramanan Rajeev and Raghavan B. Sunoj*

Department of Chemistry, Indian Institute of Technology Bombay, Powai, Mumbai 400076, India

Supporting Information

ABSTRACT: The reactions of excited state singlet molecular oxygen ($^1\Delta_g$,$^1O_2$) continue to witness interesting new developments. In the most recent manifestation, $^1O_2$ is tamed to react with enecarbamates in a stereoselective manner, which is remarkable, in view of its inherently high reactivity (*Acc. Chem. Res.* **2008**, *41*, 387). Herein, we employed the CAS-MP2(8,7)/6-31G* as well as the CAS-MP2(10,8)/6-31G* computations to unravel the origin of (i) diastereoselectivities in dioxetane or hydroperoxide formation and (ii) regioselectivity leading to a [2 + 2] cycloadduct or an ene product when $^1O_2$ reacts with an oxazolidinone tethered 2-phenyl-1-propenyl system. The computed Gibbs free energy profiles for *E*- and *Z*-isomers when $^1O_2$ approaches through the hindered and nonhindered diastereotopic faces (by virtue of chiral oxazolidinone) of the enecarbamates exhibit distinct differences. In the case of *E*-isomer, the relative energies of the transition structures responsible for hydroperoxide (ene product) are lower than that for dioxetane formation. On the other hand, the ene pathway is predicted to involve higher barriers as compared to the corresponding dioxetane pathway for *Z*-isomer. The energy difference between the rate-determining diastereomeric transition structures involved in the most favored ene reaction for *E*-enecarbamate suggests high diastereoselectivity. In contrast, the corresponding energy difference for *Z*-enecarbamate in the ene pathway is found to be diminishingly close, implying low diastereoselectivity. However, the dioxetane formation from *Z*-enecarbamate is predicted to exhibit high diastereoselectivity. The application of *activation strain model* as well as the differences in stereoelectronic effects in the stereocontrolling transition structures is found to be effective toward rationalizing the origin of selectivities reported herein. These predictions are found to be in excellent agreement with the experimental observations.

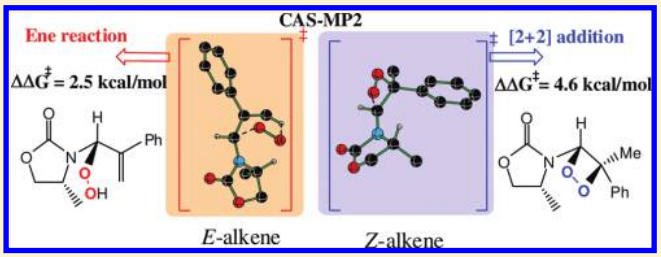

INTRODUCTION

The reactions of singlet molecular oxygen ($^1\Delta_g$) continue to remain a classic problem that attracted considerable attention from diverse scientific communities. While chemists have banked on the reactive potential of singlet oxygen toward realizing synthetically important targets,[1] biologists found interesting domains of its reactions in oxygenase enzymes and in lipid peroxidation.[2] Among the different modes of reactions with olefins, [2 + 2] cycloadditions and ene reactions are the most widely reported categories.[3] The cycloaddition reaction leads to the formation of synthetically relevant dioxetanes, whereas ene reaction is characterized by the abstraction of allylic hydrogen by the molecular oxygen resulting in a hydroperoxide.[4] The reactions of singlet oxygen with heterocyclic as well as electron rich aromatic compounds have been extensively employed in the synthesis of important compounds.[5] Over the years, the significance of singlet oxygen chemistry has provided sufficient impetus toward exploring the mechanistic details of such reactions.[6]

The major focus of mechanistic studies has been revolving around the reactions of singlet oxygen with olefins. The substrate geometry and the electronic nature of substituents on the alkene can exert a direct influence on the mechanism. A range of possibilities, as summarized in Scheme 1, has been found in the literature.[7] In a biradical stepwise mechanism, the initial C−O bond formation leads to a biradical intermediate (**1**) which could ring close to a dioxetane.[8] In a symmetry-allowed concerted [2s + 2a] addition, oxygen molecule aligns perpendicular to the alkene double bond (**2**).[9] Another symmetry allowed process goes through a perepoxide intermediate (**3**) in the initial step.[10] Single electron transfer to yield a radical cation and radical anion pair (**4**) followed by ring closure has also been proposed.[11] A charge-transfer mechanism based on the HOMO and LUMO energies of the reacting partners has been suggested to involve a symmetry-allowed [2s + 2s] process (**5**).[12] The role of electronic nature of

Scheme 1. Different Mechanistic Models for the Reaction of Singlet Oxygen with Olefin

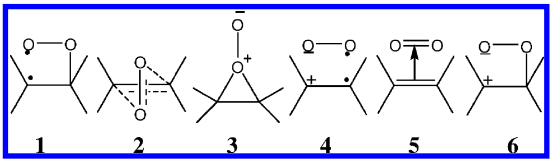

Received: January 23, 2012
Published: February 10, 2012

   dx.doi.org/10.1021/jo3001707 | *J. Org. Chem.* 2012, 77, 2474−2485

substituents, such as an amine, is suggested to be vital in steering the reaction to a zwitterionic mechanism (**6**).[13]

While successful applications of singlet oxygen chemistry are widely found in literature, stereoinduction toward generating chiral oxygenated products through this protocol remained a formidable challenge. In particular, gaining control over predictable stereochemical outcomes when dealing with an excited state molecule, such as the singlet oxygen, is a nontrivial task. Facial selectivity in singlet oxygen reactions has been previously reported using chiral motifs involving norbornyl frameworks, alkene, allylic alcohol, allylmetal systems, and so on.[14] Sivaguru, Adam, and Turro have been pioneers in *photochirogenesis*, a term describing photochemical reactions resulting in chiral induction.[15] Inspiration derived from the widespread acceptance of Evans as well as Crimmins chiral auxiliary protocols in asymmetric reactions would naturally find its extensions in photochemical reactions.[16] The most recent developments in asymmetric photochemical reactions include the use of chiral auxiliary-based stereoinduction by suitable modification of alkenes. Evans oxazolidinones tethered to olefins are reported to be efficient in asymmetric oxygenation reactions. Excellent diastereoselectivity, as shown in Scheme 2,

Scheme 2. Regio- and Stereoselectivity in the Reaction of Singlet Oxygen with Chiral Enecarbamates (ref 15)[a]

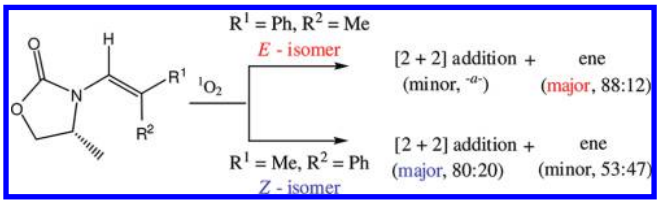

[a]Not determined.

has been reported for oxazolidinone mediated chiral induction.[15] As part of our continued efforts toward understanding the origin of chiral induction in asymmetric organic reactions,[17] we became interested in exploring this new class of asymmetric singlet oxygenation reaction. Very recently we have presented a comprehensive description of the transition structures responsible for asymmetric induction in Evans chiral auxiliary mediated aldol reactions.[18]

The asymmetric induction critically depends on the energies of the stereocontrolling transition structures. As much as the order of difficulty associated with the experimental studies on asymmetric reactions using a small molecule such as the excited-state molecular oxygen, the corresponding computational explorations are far too complicated owing to the inherent technical challenges in dealing with excited-state species. The present study focuses on the stereoselective reaction of singlet oxygen with enecarbamates leading to the formation of dioxetane and hydroperoxide. The key objectives include (i) developing a fundamental understanding of stereocontrolling elements in the vital transition structures and (ii) rationalization of regioselective preferences noticed in the reaction between an amine-activated olefin (enecarbamate) and singlet oxygen at molecular level. A schematic representation of the reaction being investigated, the regiochemical outline, and stereoselectivity are provided in Scheme 2. The results could add value to the continued legacy of singlet oxygen chemistry and help guide future progress in this domain.

COMPUTATIONAL METHODS

All of the calculations were performed using the Gaussian03 suite of quantum chemical programs.[19] Natural population analysis of the intermediates and transition structures was performed with the help of the NBO program by using the wave function obtained at the DFT(RB3LYP/6-31G*) level of theory using the Gaussian09 program.[20] The prediction of mechanism and energies of singlet oxygen reactions is often challenging. Difficulties include the lack of convergence between various mechanisms as predicted by different levels of theory. Singlet oxygen reaction with tetramethylethylene (TME) demanded the use of the CCSD(T)//RB3LYP/6-31G* level of theory toward obtaining reliable estimates of intramolecular kinetic isotopic effects.[6h] The density functional theory with Becke's three-parameter exchange functional and the gradient-corrected correlation functional of Lee, Yang, and Parr, denoted as B3LYP, were used for these calculations.[21] Earlier reports that amine activated alkenes follows a zwitterionic mechanism encouraged us to use the DFT(RB3LYP) level of theory for geometry optimizations. Pople's 6-31G* basis set was used for all the calculations. Calculations were also performed at the DFT(UB3LYP) level of theory using Noodleman's broken symmetry formalism with mixing the HOMO and LUMO.[22] For the spin contaminated saddle points spin projection method proposed by Yamaguchi et al. has been used.[23] All transition structures were fully optimized and characterized as a first-order saddle point by harmonic vibrational frequency analysis. The imaginary frequencies were first subjected to visual inspection to examine whether they represent the desired reaction coordinate in each case. Further verifications of the transition structures were carried out by using the intrinsic reaction coordinate (IRC) calculations.[24] The complete active space computations were carried out using the geometries obtained at the DFT(RB3LYP)/6-31G* level of theory. The zero-point vibrational energies, thermal as well as entropic terms obtained at the DFT(B3LYP)/6-31G* level of theory are added to the single-point energies evaluated using the CAS-MP2 methods toward obtaining the Gibbs free energies. Unless otherwise specified, Gibbs free energies are employed for discussions in this article.

Definition of the Active Space. Definition of the active space was done by carefully examining the molecular orbitals that directly take part in the reaction.[25] In the [2 + 2] mode of addition, the formation of two new σ bonds from the π-orbitals of molecular oxygen and enecarbamate takes place. The ene reaction, on the other hand, involves the formation of a new σ bond between the carbon atom and the molecular oxygen besides the abstraction of the allylic proton. Molecular orbitals of product dioxetane include both σ and σ^* orbitals of the C−O bond, allylic C−H σ and C−H σ^*.[26] Two different active spaces consisting of (a) eight electrons in seven orbitals (8,7) and (b) ten electrons in eight orbitals (10,8) have been considered in the present study. In fact, earlier reports on related studies have employed (8,7) active space for singlet oxygenation reaction.[6k] The orbitals included in the active space were as shown in Table 1.

Table 1. Molecular Orbitals Included in the Active Space

active space used	alkene	oxygen
CAS-MP2(8,7)	π C−C, π^* C−C, σ C−$H_{allylic}$, σ^* C−$H_{allylic}$	two π_g-orbitals, one π_u-orbital
CAS-MP2(10,8)	π C−C, π^* C−C, σ C−$H_{allylic}$, σ^* C−$H_{allylic}$	two π_g-orbitals, two π_u-orbitals

Higher active space is also considered for all crucial transition structures that are expected to control the regio/stereoselectivities. Additional efforts to include MP2 corrections on the energies obtained using CAS(12,10) active space (with two more orbitals, O−O σ and O−O σ^*) is found to be practically impossible to execute due to the limitation of the electronic structure suite employed in the present study.[27] Visual examination equipped with chemical intuition has been employed toward the selection of the molecular orbitals in the active space. Wherever required, orbital swapping was done to include the right choice of orbitals in the active space. Moreover, the occupation

dx.doi.org/10.1021/jo3001707 | J. Org. Chem. 2012, 77, 2474−2485

number of these active space orbitals was checked by examining the diagonal elements of the density matrix to ensure that the active space holds good throughout the calculations. This analysis indicated that all the MOs in the active space consist of occupancies between zero and two throughout the calculations until MCSCF convergence is achieved. The dynamic electron correlations were included by using the CAS-MP2 method. This approach has been successfully employed earlier toward predicting the reaction energies.[28] In the present study, CAS-MP2 is an affordable and adequate level of theory in view of the size of molecules as well as the numerous possibilities that were required to be considered in arriving at meaningful conclusions.

RESULTS AND DISCUSSION

A comprehensive mechanistic investigation on various pathways involved in the addition of singlet oxygen to *E*- and *Z*-enecarbamate, as shown in Scheme 2, is undertaken by using density functional theory (RB3LYP and UB3LYP) as well as complete active space calculations including second-order Møller−Plesset perturbative terms (CAS-MP2). Detailed analysis of the energies, geometries of the intermediates, and the interconnecting transition structures are carried out to account for the reported product selectivity of the title reaction. Computed relative energies of the stationary points are employed to rationalize the observed regioselectivity and the stereoselectivity of singlet oxygenation reaction.

The addition of singlet oxygen to olefins and the accompanying mechanistic possibilities have been extensively documented, particularly in regard to the type of intermediates involved in the reaction pathway.[5] The oxygen molecule can react with alkenes either in a [2 + 2] mode of cycloaddition resulting in the formation of dioxetane or proceed through an ene reaction pathway which involves the abstraction of an allylic hydrogen leading to a hydroperoxide product. It is reported that though [2 + 2] cycloaddition can proceed in a concerted or a stepwise fashion, which are directly influenced by the electronic nature as well as the orientation of the substituents around the double bond in alkenes. Majority of reports support a stepwise mechanism proceeding through a perepoxide intermediate.[7b,d,f,h] The stabilization of ensuing intermediates could play a major role toward determining whether the reaction proceeds through a stepwise or a concerted pathway. While the chemistry of singlet oxygen remained in the forefront for many years, stereocontrol in asymmetric oxygenations with the help of chiral auxiliaries is accomplished only very recently.[15,16] The *E* and *Z* diastereomers of an enecarbamate, consisting of a chiral oxazolidinone, can offer facially different environments to the incoming oxygen molecule, owing to the cumulative differences in steric, electronic, and potential weak interactions. The differing steric environments prevailing on the diastereotopic faces of the olefinic bond might lead to changes in the mechanistic course of the reaction. Additionally, orientation of the incoming oxygen molecule with respect to the chiral auxiliary can give rise to a *syn* or *anti* alignment of addition.[29] Stereochemical outcome of the reaction will depend on many/all of these factors; delineation of the same forms the premise for the present investigation. In the lower energy conformer of enecarbamate used in the present study, the oxazolidinone ring is found to be coplanar with the olefin. Another rotamer arising due to the rotation around the C−N bond is found to be of higher energy.[30] Therefore, the lower energy isomer, as shown in Scheme 2, is considered for further study.

For sake of clarity, the discussions are broadly grouped into three sections, such as the mechanistic possibilities and stereoselectivity issues involved in the addition of singlet oxygen to (i) *E*-enecarbamate, (ii) *Z*-enecarbamate, and (iii) the pathway involving the conversion of dioxetane to hydroperoxide.

(a). Addition of Singlet Oxygen to *E*-Enecarbamate. Different stereochemical possibilities for the [2 + 2] addition of $^1O_2$ to *E*-enecarbamate leading to the formation of dioxetane are provided in Scheme 3. Besides the differences in the facial

Scheme 3. Mechanistic Possibilities for the Formation of Dioxetane through [2 + 2] Addition between Molecular Oxygen and *E*-Enecarbamate

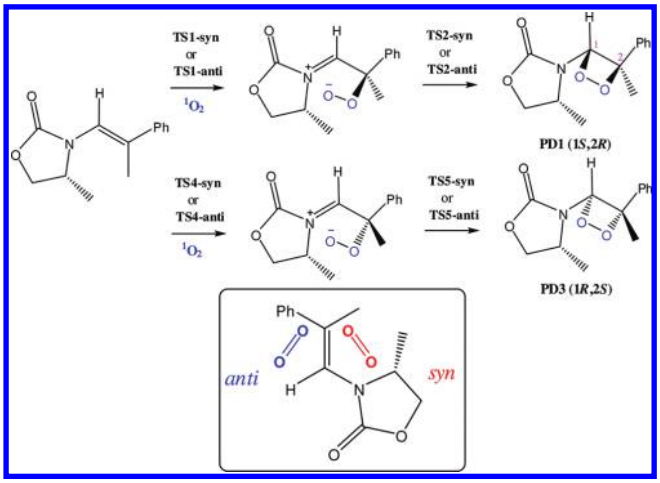

approaches, molecular oxygen can align in two key orientations in each face of the enecarbamate, as shown in the inset (Scheme 3). The approach of $^1O_2$ with one of the oxygen atoms pointing toward the nitrogen of the oxazolidinone is termed as *syn*, while the other orientation wherein the oxygen atom is farther is termed as *anti*. These stereochemical possibilities collectively open up four key pathways toward the formation of two diastereomeric products as depicted in Scheme 3.

First, both *syn* and *anti* orientations are identified for the approach of oxygen molecule to the less hindered face of the enecarbamate. The Gibbs free energy profile for the formation of two diastereomeric products is summarized in Figure 1.[31] It can be readily noticed that the pathway wherein the oxygen molecule is aligned *anti* is higher in energy than the *syn* addition. Columbic repulsion between the incoming oxygen and the nitrogen of the oxazolidinone is found to have a direct bearing on the predicted energy difference. For instance, the O1−N1 distance in the higher energy **TS1-anti** is shorter (2.43 Å) than that in **TS1-syn** (2.69 Å), implying the presence of a higher Columbic repulsion in the former case (Figure 2).[32]

The optimized geometries of the key transition structures are provided in Figure 2. Examination of the geometric features of the lowest energy **TS1-syn** indicates an early transition structures. In particular, C2−O2 (1.80 Å), and O1−O2 (1.30 Å) distances as well as the angles around C2 (sum of angles subtended by all three bonds around the trigonal carbon is 357.34°, implying a degree of pyramidalization of 2.66°) are characteristic of an early TS.[33] The incipient C2−O2 bond distance representing the key change along the reaction coordinate is 1.80 Å. Another important feature of **TS1-syn** relates to the charge distribution reminiscent of a polar species. The natural charges on O1(−0.38) and O2(−0.15) exhibit a

dx.doi.org/10.1021/jo3001707 | J. Org. Chem. 2012, 77, 2474−2485

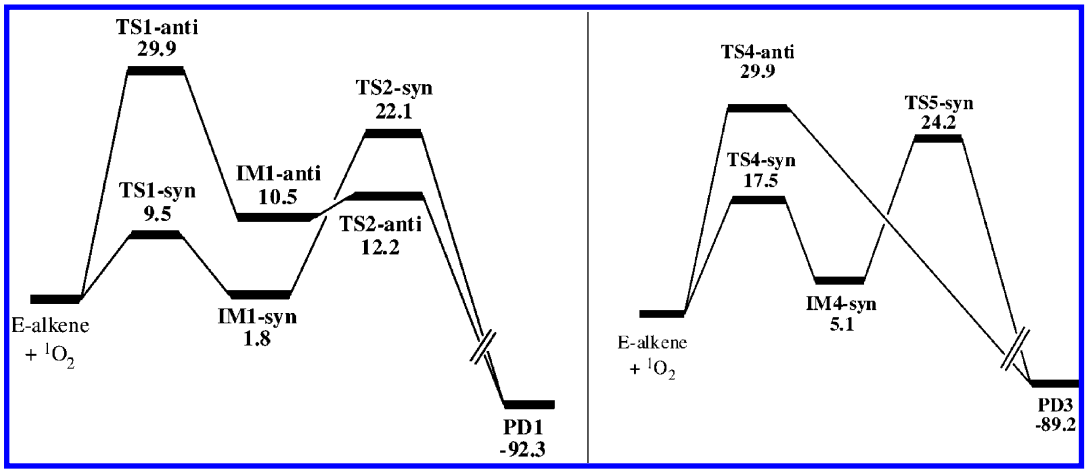

Figure 1. Free energy diagrams for the formation of diastereomeric dioxetanes from *E*-enecarbamate through [2 + 2] cycloaddition. The relative free energies (in kcal mol^{-1}) are obtained at the CAS-MP2(8,7)/6-31G*//RB3LYP/6-31G* level of theory.

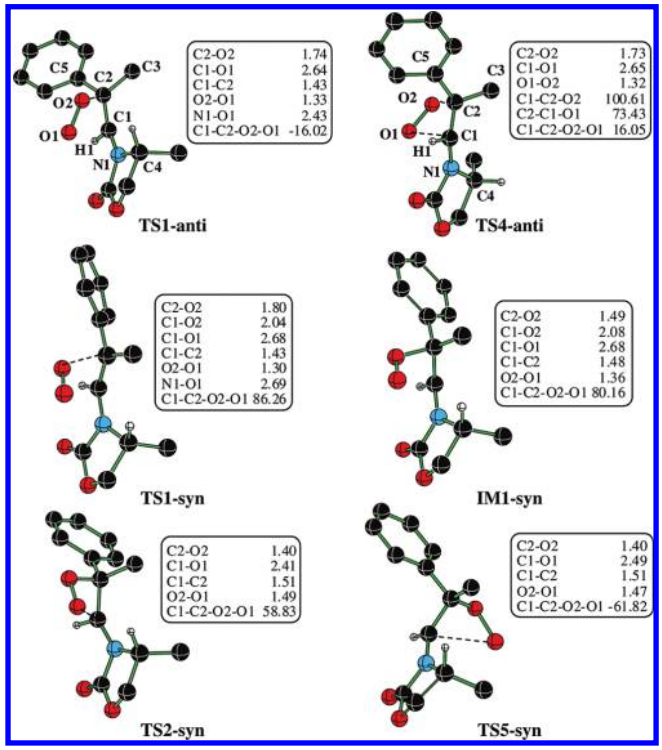

Figure 2. Representative geometries of transition structures and intermediate optimized at the DFT(RB3LYP/6-31G*) level of theory for the addition of molecular oxygen to *E*- enecarbamate (distances are given in angstroms and angles in degrees).

considerable difference.[34] The transition structure **TS1-syn** leads to a polar and thermodynamically stable intermediate **IM1-syn**. The natural charges on O1 and O2 of **IM1-syn** are, respectively, −0.46 and −0.19. The newly formed C2−O2 bond distance is about 1.40 Å. Interestingly, C1−O2 distance of 2.08 Å in **IM1-syn** could be regarded as a weak epoxidic linkage. The dihedral C2−C1−O2−O1 is 80.2°, which suggests that the molecular oxygen remains nearly perpendicular to the previous double bond position. The structural and electronic features of the transition structure and the intermediate are in concurrence with a previous report, by Dewar and Thiel, that amine activated alkenes tend to exhibit an ionic mechanism as opposed to a radical mechanism.[13]

Next, the ring closure in **IM1-syn** occurs by C1−O1 bond formation through **TS2-syn**. The present prediction that the dioxetane formation through [2 + 2] mode of addition involves a two-step mechanism is along similar lines to that of singlet oxygenation with amine-activated olefins.[13] However, the barrier for the elementary step for the ring closure is identified as the rate determining step unlike the initial addition (C2−O2 bond formation) suggested before for related substrates. Interestingly, in the case of unactivated olefins, the rate-determining step is reported to be the second step leading to ring closure. It is important to note that the changes in the stereoelectronic environment of the enecarbamate due to the tethered oxazolidinone, as compared to a simpler amine-activated analogue, can impart a pronounced effect in the overall energetics of singlet oxygen addition. The ability of amido nitrogen in oxazolidinone to delocalize the lone pairs renders improved stabilization to **IM1-syn**.[35]

The stereochemical outcome in the dioxetane formation can be explained by comparing the facially discriminating steps. It is evident from the Figure 1 that the approach of molecular oxygen through the hindered face (**TS4-syn**) is of higher than through the less hindered face (**TS1-syn**). The highest energy points on the lower energy pathways for the addition to both diastereotopic faces of enecarbamate are considered for a detailed comparison. The corresponding transition structures for the addition to the less hindered face is **TS2-syn** and that on the hindered face is **TS5-syn**. A difference of 2.1 kcal mol^{-1} between the relative energies of these transition structures suggests a diastereomeric excess to the tune of 94%.[36] This vital energy difference is rationalized by comparing the stabilizing and destabilizing interactions operating in these transition structures. More favorable interactions are identified in **TS2-syn**. The key geometric differences between **TS2-syn** and **TS5-syn** are (i) the incipient C1−O1 bond distances, which are, respectively, 2.41 and 2.49 Å, indicating a more effective orbital overlapping in the former case (furthermore, O1−O2 distances suggest a better delocalization between the olefin and oxygen molecule in **TS2-syn** (1.49 Å) as compared to **TS5-syn** (1.47 Å)), and (ii) the proximity between the lone pair electrons on the terminal oxygen and the filled orbitals of the methyl group of oxazolidinone, which evidently is closer in **TS5-syn** implying an enhanced repulsion.[37]

In addition to the above-mentioned geometric origins to the relative energy differences, the subtle changes in stereo-

dx.doi.org/10.1021/jo3001707 | J. Org. Chem. 2012, 77, 2474−2485

electronic effects in these transition structures have been further probed with the help of *activation strain model*.[38] The constituent reactants in the transition structures are first separated into two fragments, namely the molecular oxygen and the enecarbamate. The deformation and interaction energies with respect to the lower energy transition structure are summarized in Table 2. The deformation of both oxygen and

Table 2. Summary of Activation Strain Analysis of the Transition Structures for [2 + 2] Cycloaddition between $^1O_2$ and *E*-Enecarbamate (Relative Deformation and Interaction Energies[a] of Fragments Provided in kcal mol^{-1})

	deformation energy		
transition structures	$^1O_2$	enecarbamate	interaction energy
TS2-syn	1.7	3.5	−7.6
TS5-syn	0.0	0.0	0.0

[a]Relative energies are defined with respect to the fragments of higher energy **TS5-syn**.

the enecarbamate energy in **TS5-syn** is found to be higher by 5.2 kcal mol^{-1} than that in **TS2-syn**. However, the compensation arising through a better interfragment interaction in **TS2**-syn is responsible for higher stabilization of **TS2-syn.** Interaction energy in **TS2-syn** is 7.6 kcal mol^{-1} higher as compared to that in **TS5-syn**. This conveys that the interaction contributes to the observed energy difference than the distortion in individual reacting fragments.

As discussed earlier, another possible orientation for the incoming oxygen molecule is to remain *anti* with respect to the oxazolidinone nitrogen.[39] Similar to the trends noticed with the approach to the less hindered face, *anti* orientation for the addition to the hindered face is also found to be of higher energy. Here, transition structure **TS4-anti** is highly asynchronous and concerted.[40] The optimized geometry of the transition structure for the corresponding addition, **TS4-anti** is provided in Figure 2. The distances between carbon and oxygen, C1−O1 and C2−O2 are, respectively, 2.65 Å and 1.73 Å.

The discussions thus far have been centered around the [2 + 2] cycloaddition of singlet oxygen to the enecarbamate. Another competitive pathway known to be important in singlet oxygen reactions is the ene reaction, wherein the terminal oxygen atom abstracts one of the allylic hydrogens to furnish a hydroperoxide product as shown in Scheme 4.

Our calculations at the DFT(RB3LYP) level of theory reveal that the ene reaction proceeds in a single step which includes the formation of a new carbon oxygen bond as well as the abstraction of a proton from the allylic position. It appears evident that an amine-activated olefin exhibits significant mechanistic variations as compared to simpler olefins. The recent computational study by Acevedo and co-workers on the ene reaction of tetramethylethylene indicated the participation of a symmetric charge-separated perepoxide intermediate.[41] In keeping with the literature precedence, we have carried out additional computations using the unrestricted formalism at the DFT(UB3LYP)/6-31G* level of theory. The DFT(UB3LYP) level predicts that the reaction proceeds through a stepwise mechanism involving a diradicaloid intermediate. Similar situations where the singlet oxygen ene reaction involves a stepwise or concerted mechanism have been reported wherein DFT(RB3LYP) predicted a concerted pathway while DFT-(UB3LYP) identified a stepwise mechanism (ref 6h). The results of the DFT(UB3LYP) calculations are summarized in Scheme 5 and Table 3.

The geometries of the corresponding transition structures obtained at the DFT(RB3LYP)/6-31G* level of theory is provided in Figure 3. The relative free energy of transition structure for the ene reaction (**TS3**) with respect to the separated reactants is 20.6 kcal mol^{-1} at the CAS-MP2(8,7) level of theory. Interesting comparisons can be drawn between the ene and dioxetane pathways. For instance, the preferred site of attack by the singlet oxygen is respectively at C1 and C2 atoms for [2 + 2] and ene pathways. The comparison of **TS3** with **TS2-syn** of relative energy 22.1 kcal mol^{-1} which is the rate determining step in [2 + 2] addition is in line with the reported regioselectivity in favor of the ene product in the case of *E*-isomer.[15] Although, the ene reaction is generally believed to be a barrierless process, Houk et al. has showed by using the CAS-MP2/UB3LYP calculations on a *trans* cyclooctene that strained transition structures could exhibit a finite barrier toward the conversion to ene product.[6k]

The approach of singlet oxygen through both the diastereotopic faces of the enecarbamate is examined. The relative free energies of the corresponding diastereomeric transition structures **TS3** and **TS6** at the CAS-MP2(8,7)/6-31G*//RB3LYP/6-31G* level of theory are, respectively, found to be 20.6 and 23.1 kcal mol^{-1}. Calculated energies at higher active space of (10,8) also predict the energies in similar way as 17.8 and 25.9 kcal mol^{-1}. Such large differences evidently indicate a strong facial preference, in favor of the

Scheme 4. Ene Reaction of Molecular Oxygen with *E*-Enecarbamate

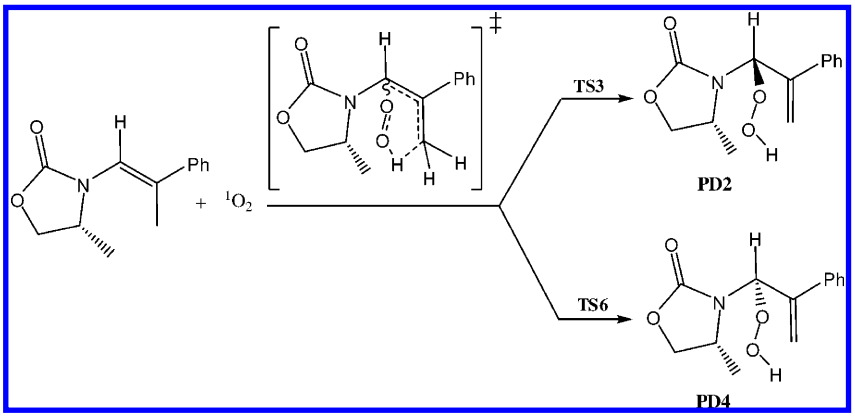

dx.doi.org/10.1021/jo3001707 | J. Org. Chem. 2012, 77, 2474−2485

Scheme 5. Stepwise Pathway for Ene Reaction of *E*-Enecarbamate Obtained Using the DFT(UB3LYP) Level of Theory

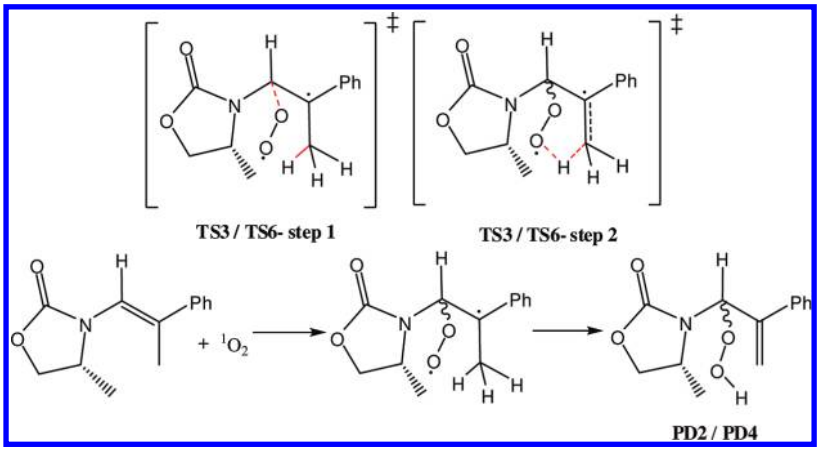

Table 3. Relative Energies (in kcal mol^{-1}) Obtained at the DFT(UB3LYP)/6-31G* Level of Theory for Ene Reaction[a]

	TS3	TS6
step 1	8.4/*8.4*	11.8/*11.8*
step 2	4.6/*3.5*	6.5/*4.9*

[a]Values in italics are the corrected final energies for spin contamination.

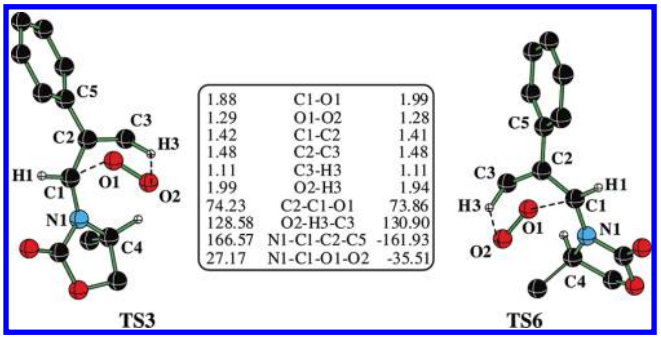

Figure 3. Geometries of the transition structures optimized at the DFT(RB3LYP)/6-31G* level of theory for the ene reaction of *E*-enecarbamate (distances are given in angstroms and angles in degrees).

product originating from **TS3**.[42] The examination of geometric features of these diastereomeric transition structures indicates considerable differences in the incipient C1−O1 bond distances (Figure 3). The C1−O1 distances are respectively found to be 1.88 Å and 1.99 Å in **TS3** and in **TS6**. The disposition of the methyl group at the chiral center of the oxazolidinone ring (C4) in **TS6** toward the incoming dioxygen obviously leads to relatively higher repulsive interaction and results in reduced efficiency of primary orbital interaction responsible for the C1−O1 bond formation. The key dihedral angle N1−C1−O1−O2 in transition structures **TS3** and **TS6** are, respectively, found to be 27.17° and −35.5° indicating a change in the orientation of the dioxygen due to differing steric interactions. The activation strain analysis as shown in Table 4 indicates that the molecular oxygen in **TS3** suffers slightly higher deformation (1.3 kcal mol^{-1}) as compared to that in **TS6**. However, the interaction energy in **TS3** is found to be better (4.4 kcal mol^{-1}) than that in **TS6**. The cumulative effect of above-mentioned stereoelectronic factors makes **TS6** of higher energy as compared to **TS3**.[43]

Table 4. Summary of Activation Strain Analysis of the Transition Structures Involved in Singlet Oxygen Ene Reaction (Relative Deformation and Interaction Energies[a] of Fragments Provided in kcal mol^{-1})

	deformation energy		
transition structure	$^1O_2$	enecarbamate	interaction energy
TS3	1.3	−0.3	−4.4
TS6	0.0	0.0	0.0

[a]Relative energies are defined with respect to the fragments of higher energy **TS6**.

(b). Addition of Singlet Oxygen to *Z*-Enecarbamates.

The reaction of singlet oxygen with another diastereomer of the enecarbamate, namely the *Z* isomer, is studied. The formation of dioxetane through [2 + 2] cycloaddition between oxygen molecule and *Z*-enecarbamate is given in Scheme 6. Akin to *E*-enecarbamate presented earlier, two regiochemical and two stereochemical possibilities for *Z*- enecarbamate are also examined.

The Gibbs free energy profiles for the formation of two diastereomeric products arising from the above-mentioned pathways are summarized in Figure 4.[44] Similar to *E*-enecarbamate, the *anti* addition transition structures (**TS7-anti** and **TS10-anti**) are of higher energy as compared to the corresponding *syn* addition. A stepwise process is identified for both *syn* and *anti* orientations of the oxygen molecule when addition is through the less hindered face of the enecarbamate. Interestingly, when the oxygen approaches through the hindered face only the *syn* addition proceeds in a stepwise mechanism while the *anti* addition involves a highly asynchronous and concerted transition structure.[45] Geometries of the key transition structures obtained at the DFT (RB3LYP)/6-31G* level of theory are given in Figure 5.

TS7-anti is the highest energy transition structure for the *anti* addition through the less hindered face and **TS10-anti** for the addition to the hindered face. The key distances such as C1−O1 and C2−O2 are, respectively, found to be 2.62 Å and 1.73 Å in **TS10-anti**. The dihedral angle between the molecular oxygen and the double bond in enecarbamate as represented by the C1−C2−O2−O1 is 5.25°. The degree of pyramidalization at C2 is 13.2°. Tethered oxazolidinone is found to be effective toward imparting facial discrimination, which holds the key to high stereoselectivity. The transition structure for the initial approach of the molecular oxygen through the less hindered

dx.doi.org/10.1021/jo3001707 | *J. Org. Chem.* 2012, 77, 2474−2485

Scheme 6. Mechanistic Possibilities for the Formation of Dioxetane through [2 + 2] Addition between Oxygen Molecule and *Z*-Enecarbamate

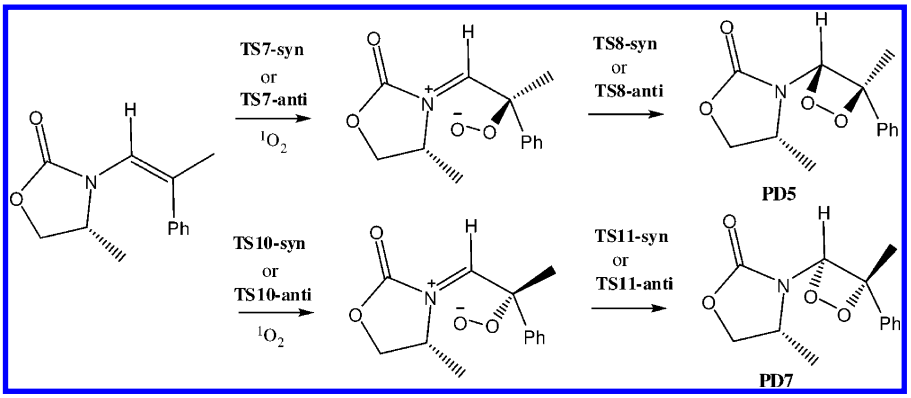

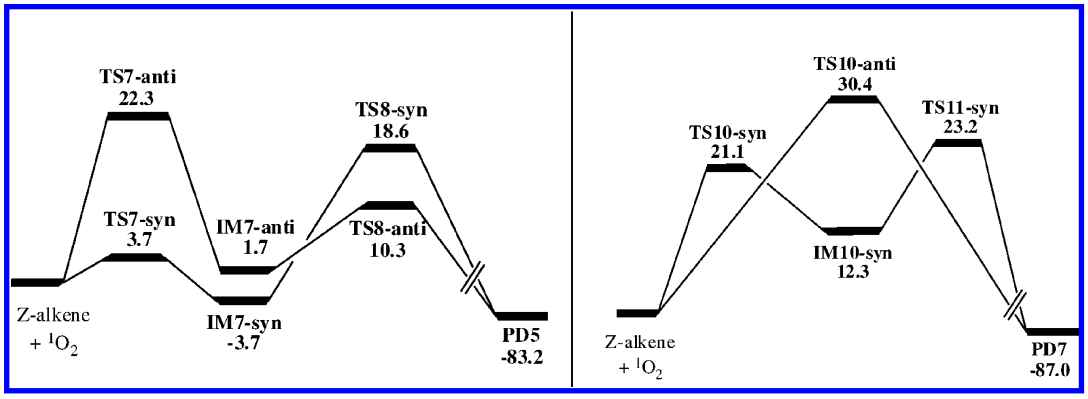

Figure 4. Free energy diagrams for the formation of diastereomeric dioxetanes from *Z*-enecarbamate through [2 + 2] cycloaddition. The relative free energies (in kcal mol^{-1}) are obtained at the CAS-MP2(8,7)/6-31G*//RB3LYP/6-31G* level of theory.

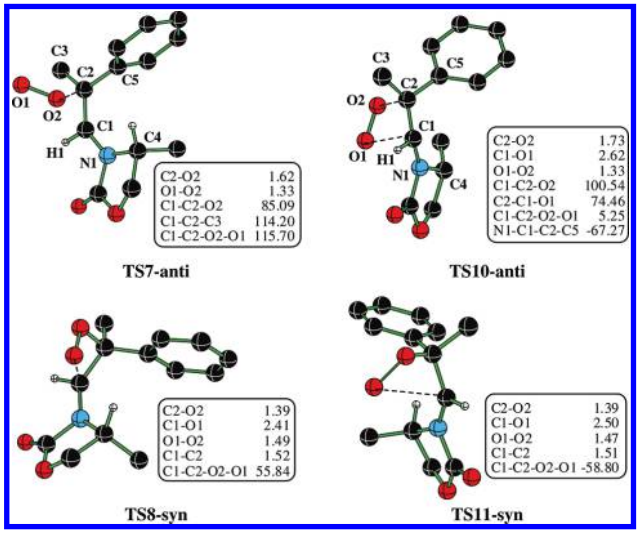

Figure 5. Representative geometries of transition structures optimized at the DFT(RB3LYP)/6-31G* level of theory for the addition of molecular oxygen to *Z*-enecarbamate (distances are given in angstroms and angles in degrees).

face (**TS7-syn**) is found to be much lower in energy than the corresponding transition structure **TS10-syn** through the hindered face. The energy difference between the highest energy transition structures on the lowest energy pathways, (i.e., **TS8-syn** and **TS11-syn**) for the approach of molecular oxygen to both the diastereotopic faces are considered for computing the diastereoselectivity. Furthermore, **TS8-syn** is the rate-determining transition structure for the approach of the oxygen molecule through the less hindered face of the enecarbamate while **TS11-syn** represents that through the hindered face. The relative energy of **TS8-syn** (18.6 kcal mol^{-1}) is found to be lower than **TS11-syn** (23.2 kcal mol^{-1}). A difference in the relative energy, as large as 4.6 kcal mol^{-1}, is in good accord with the experimentally reported stereoselectivity of >98:2 of **PD5** over **PD7**.[15]

The optimized transition structure geometry of **TS8-syn** reveals a better primary orbital overlap leading to the formation of the new σ bonds. The C1−O1 distance in **TS8-syn** is 2.41 Å while that in **TS11-syn** is 2.50 Å. These geometrical features convey that the molecular oxygen is closer to the double bond in **TS8-syn** than in **TS11-syn**. Improved delocalization leading to higher $\pi^*_{O=O}$ population in **TS8-syn** is further evident from the O═O distances in **TS11-syn**. In the case of **TS11-syn**, the methyl group at the chiral center of oxazolidinone points toward the incoming molecular oxygen, as shown in Figure 5. This situation can evidently cause relatively higher electrostatic repulsion between lone pairs of oxygen with the filled C−H bond pairs. Furthermore, the *activation strain* analysis (Table 5) reveals a relatively better interaction between the enecarbamate and the molecular oxygen in **TS8-syn** (8.9 kcal mol^{-1}) as compared to that in **TS11-syn**. However, the distortion energy of **TS8-syn** is found to be higher than in **TS11-syn** by 6.4 kcal mol^{-1}. The cumulative stabilization in the case of **TS8-syn** is higher owing to better interaction energy. All the above-mentioned stereoelectronic terms justify why **TS8-syn** is the lowest energy transition structure leading to dioxetane.

dx.doi.org/10.1021/jo3001707 | *J. Org. Chem.* 2012, 77, 2474−2485

Table 5. Summary of Activation Strain Analysis of the Transition Structures for [2 + 2] cycloaddition between $^1O_2$ and *Z*-Enecarbamate (Relative Deformation and Interaction Energies[a] of Fragments Provided in kcal mol^{-1})

	deformation energy		
transition structure	$^1O_2$	enecarbamate	interaction energy
TS8-syn	2.7	3.7	−8.9
TS11-syn	0.0	0.0	0.0

[a]Relative energies are defined with respect to the fragments of higher energy **TS11-syn**.

Next, a potential competitive pathway open to singlet oxygenation reaction is examined. As described previously, the ene reaction involves the abstraction of one of the allylic hydrogens by the terminal oxygen leading to the formation of a hydroperoxide, as shown in Scheme 7. Results of DFT-(UB3LYP) calculations are summarized in Scheme 8 and Table 6. Akin to *E*-isomer, *Z*-isomer also exhibited a stepwise mechanism at the DFT(UB3LYP) level of theory.

The transition structure for the addition of singlet oxygen to the less hindered face (as seen by the orientation of the methyl group at the chiral center of the oxazolidinone ring) is termed as **TS9** while that for the hindered face is **TS12**.

The computed energetics offers interesting connections with the reported experimental observations. First, the relative energies of both the diastereomeric transition structures for the ene reaction of *Z*-enecarbamate is found to be very close at both DFT(RB3LYP)/6-31G* and the CAS-MP2 levels of theory. The relative free energies of **TS9** and **TS12** computed at the CAS-MP2(10,8) level of theory are, respectively, found to be 19.1 and 19.4 kcal mol^{-1}, implying only a negligible stereoselectivity. In fact, this prediction is in excellent agreement with the reported diastereomeric ratio of **PD6** to **PD8** which is 53:47.[15] Computations using the lower active space, such as the CAS-MP2(8,7)/6-31G*//RB3LYP/6-31G* similarly yields only a marginal difference in energies between **TS9**(16.9) and **TS12**(16.5 kcal mol^{-1}). Another important aspect relates to the comparison of the relative energies of the rate determining transition structures in [2 + 2] mode of addition (**TS8-syn**, 6.6 kcal mol^{-1}) with that for the ene reaction (**TS9**, 7.6 kcal mol^{-1}). This energetic trend conveys a preferred formation of dioxetane over ene product. These predictions are in concert with the experimental observation that *Z*-enecarbamate furnishes dioxetane as the major product than ene products.[15] However, the free energy estimates at the CAS-MP2(10,8)/6-31G*//RB3LYP/6-31G* level is found to be inconsistent with the experimental observation. This is the only instance of a minor discrepancy between the computed electronic energy and Gibbs free energy, where **TS8-syn** is found to be 0.5 kcal mol^{-1} higher in energy than **TS9**. A comparison of energies all crucial transition structures are summarized in Table 7.

The geometries of the key transition structures involved in the ene reaction of *Z*-enecarbamate is provided in Figure 6. The chairlike geometry is noticed for both **TS9** and **TS12** which corresponds to C1−O1 bond formation as well as the abstraction of the allylic proton. The allylic hydrogen that is being abstracted (C3−H3, 1.13 Å in **TS9**) is elongated in the transition structure as compared to other allylic hydrogens (1.09 Å). The IRC calculations reveal that the transition structure geometry connects smoothly to the ene product in a single step.[46]

(c). Conversion of Dioxetane to Hydroperoxide. In addition to the direct formation of the ene products, an alternative pathway for the conversion of the initially formed dioxetane to the ene product is also examined (Scheme 9). In this pathway, C2−O2 bond of dioxetane opens up and subsequent abstraction of one of the methyl hydrogens leads to the ene product. The examination of the IRC trajectories suggests a single step mechanism, without the involvement of any intermediate for this conversion.

The transition structures for the conversion of four key dioxetane diastereomers to ene products, denoted as **TS13**, **TS14**, **TS15**, and **TS16**, are located. The conversion of dioxetane to ene product is found to involve a relatively higher barrier, readily suggesting that the pathway is less likely to operate. For instance, **TS15** for dioxetane to hydroperoxide conversion is found to be 8 kcal mol^{-1} higher in energy at the DFT (RB3LYP)/6-31G* level of theory than the direct formation of hydroperoxide through an ene transition structure, say **TS3**. The transition structures geometries, as given in Figure 7, exhibit a strained four-membered ring constituted by O2, H3, C3, and C2 atoms in an overall boat-like conformation. In the case of corresponding direct ene reaction a chairlike geometry is identified. The reaction coordinates consist of relative atomic displacements involving four atoms (O2, H3, C3, and C2). The energies of all these transition structures (**TS13**-**TS16**) are within the range of a kcal mol^{-1}.

Scheme 7. Ene Reaction of Molecular Oxygen with *Z*-Enecarbamate

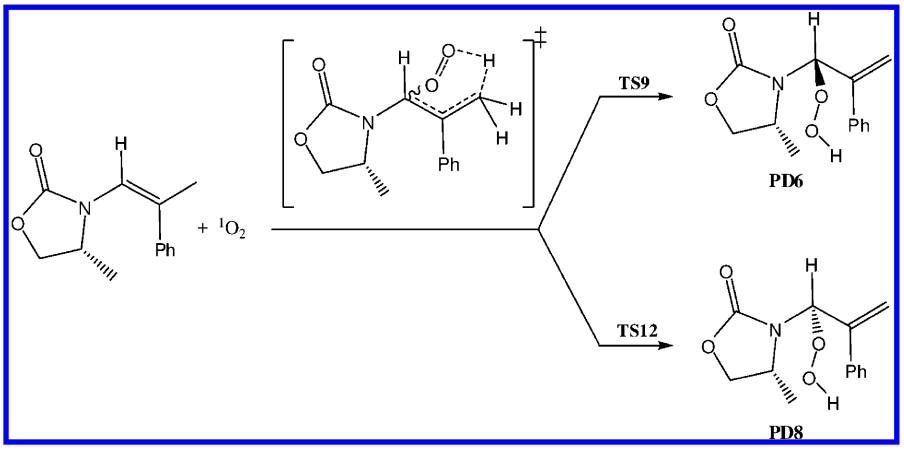

dx.doi.org/10.1021/jo3001707 | J. Org. Chem. 2012, 77, 2474−2485

Scheme 8. Stepwise Pathway Predicted by DFT(UB3LYP)/6-31G* Level of Theory for Ene Reaction for *Z*-Enecarbamate

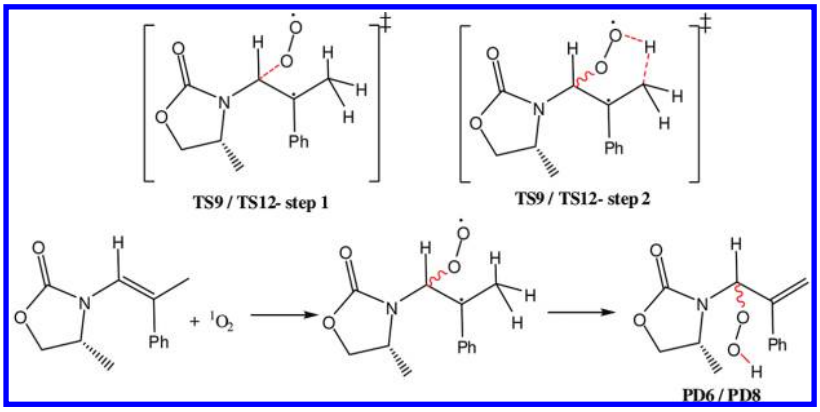

Table 6. Relative Energies (in kcal mol^{-1}) Obtained at the DFT(UB3LYP)/6-31G* Level of Theory for Ene Reaction[a]

	TS9	TS12
step 1	8.1/*10.5*	8.3/*9.9*
step 2	9.5/*7.9*	11.6/*9.8*

[a]Values in italics are the corrected final energies for spin contamination.

Finally, a direct comparison between the computed relative energies and its implications to the experimentally reported product selectivity is presented. A comparison of relative free energies obtained at the higher active space of CAS-MP2(10,8) with that obtained using the lower active space of CAS-MP2(8,7) is as well presented. To fulfill this objective a summary of the key findings are collected in Table 7. Interestingly, both active spaces yielded mutually consistent results. The relative energies of the transition structures on the minimum energy pathway, leading to dioxetane and ene products from both the diastereotopic faces of enecarbamates, are provided. In the case of *E*-enecarbamate, it can be readily noticed that **TS3** for ene reaction is lower in energy (by 1.5 kcal mol^{-1}) than **TS2-syn** for [2 + 2] cycloaddition, indicating a clear regiochemical preference toward ene reaction. Interestingly, the product distribution in the case of *E*- enecarbamate is reported to be predominantly in favor of ene product, with a ratio of 16:84.[15] More importantly, the high diastereoselectivity of the ene product, computed on the basis of the energy difference between **TS3** and **TS6**, is in excellent agreement with the experimental ratio of 88:12 (in favor of 1*S* product). In a similar fashion, the regiochemical reversal for the site of oxygen addition when the enecarbamate is in the *Z*-configuration could as well be effectively rationalized. The electronic energy of **TS8-syn** is lower than that of **TS9**, clearly indicating a preference toward [2 + 2] cycloaddition over ene pathway. Again, the origin of high diastereoselectivity in dioxetane formation is traced to the large energy difference between the transition structures for the addition of $^1O_2$ respectively to nonhindered (**TS8-syn**) and hindered (**TS11-syn**) faces. The poor diastereoselectivity (53:47 1*S*:1*R*) noticed in the ene product is identified as arising due to the diminishingly closer energies between the corresponding transition structures (**TS9** and **TS12**).

CONCLUSIONS

The different mechanistic possibilities for the addition of excited state singlet molecular oxygen to a chiral enecarbamate consisting of oxazolidinone have been investigated by using the density functional and CAS-MP2 level of theories. Closed-shell spin restricted calculations involving a zwitterionic mechanism and open-shell spin unrestricted calculations through a diradicaloid pathway have been considered. The predictions on the basis of the spin restricted zwitterionic pathway have been found to in good agreement with the experimental reports. The approach of $^1O_2$ through both diastereotopic faces of *E*- and *Z*-enecarbamate has been examined. The lower energy pathways for the formation of dioxetane and hydroperoxide are established. In most cases, the [2 + 2] cycloaddition mode is found to proceed through a stepwise pathway involving polar zwitterionic intermediates wherein the second C−O bond formation is the rate determining step. The important regio- and diastereochemical preferences predicted

Table 7. Relative Energies and Free Energies (in kcal mol^{-1}) of Crucial Transition Structures for $^1O_2$ Addition to Enecarbamate[a] at Different Level of Theories

isomer	transition structure	face of $^1O_2$ approach	*L1*	*L2*	*L3*	computed regio-/stereoselectivity	exptl regio-/stereoselectivity
E-alkene	**TS2-syn**	nonhindered	22.1	20.6	7.9	ene (1*S*)	ene (1*S*)
	TS5-syn	hindered	24.2	28.9	16.0		
	TS3	nonhindered	20.6	17.5	4.5		
	TS6	hindered	23.1	25.9	13.5		
Z-alkene	**TS8-syn**	nonhindered	18.6	19.6	6.6	dioxetane[b] (1*S*,2*S*)	dioxetane (1*S*,2*S*)
	TS11-syn	hindered	23.2	26.1	13.0		
	TS9	nonhindered	16.8	19.1	7.6		
	TS12	hindered	16.5	19.5	8.5		

[a]*L1*: Gibbs free energies at the CAS-MP2(8,7)/6-31G*//RB3LYP/6-31G*. *L2*: Gibbs free energies at the CAS-MP2(10,8)/6-31G*//RB3LYP/6-31G*. L3: Electronic energies at the CAS-MP2(10,8)/6-31G*//RB3LYP/6-31G*. [b]Regioselectivity of dioxetane is better reproduced by *L3*.

dx.doi.org/10.1021/jo3001707 | *J. Org. Chem.* 2012, 77, 2474−2485

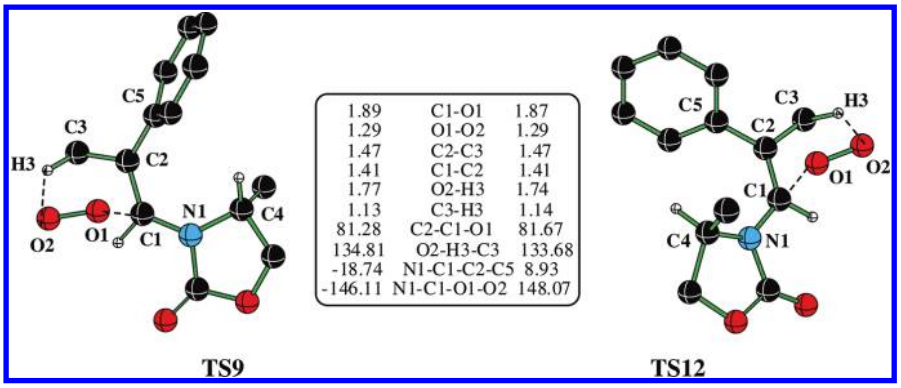

Figure 6. Geometries of the transition structures optimized at the DFT(RB3LYP)/6-31G* level of theory for the ene reaction of *Z*-enecarbamate (distances are given in angstroms and angles in degrees).

Scheme 9. Direct Conversion of Dioxetane Obtained from *E*-Enecarbamate as Well as *Z*-Enecarbamate to the Corresponding Hydroperoxides

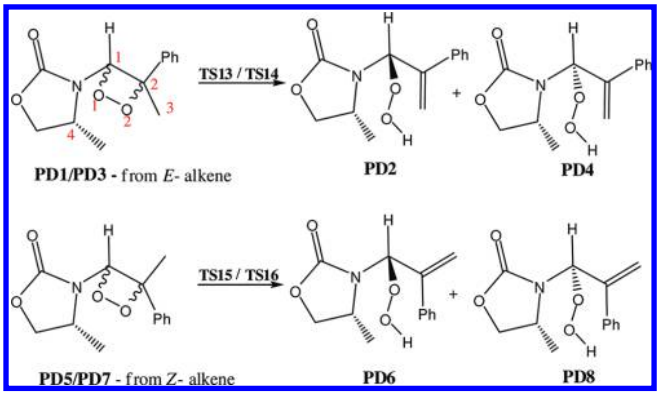

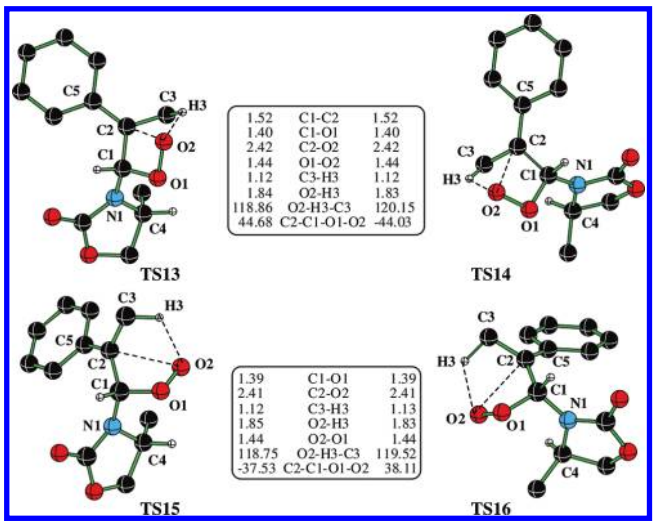

Figure 7. Geometries of the transition structures optimized at the DFT(RB3LYP)/6-31G* level of theory for the conversion of dioxetane to hydroperoxide.

on the basis of the relative energies of key transition structures are (i) the preferred site of $^1O_2$ addition exhibits a strong regiochemical bias toward the ene pathway in the case of *E*-enecarbamate while dioxetane formation is preferred in *Z*-enecarbamate, (ii) high diastereomeric excess for the ene product for *E*-enecarbamate and dioxetane cycloadduct for *Z*-enecarbamate, and (iii) poor diastereoselectivity in the minor ene product in *Z*- enecarbamate. Computed regiochemical reversal noticed between *E* and *Z* enecarbamate is in concurrence with the earlier experimental report that the *E*-enecarbamate offers ene product while *Z*-enecarbamate yields dioxetane product. The factors responsible for high diastereoselectivity have been traced to the differential stereoelectronic effects in the competing transition structures. The interaction between the reactants as well as the geometric distortions in the transition structures as compared to the corresponding ground state species, analyzed within the framework of the *activation strain model* has also been effective in rationalizing the energetic ordering between competing diastereomeric transition structures.

■ ASSOCIATED CONTENT

Ⓢ Supporting Information

Optimized geometries for all the stationary points, total electronic energies, description of the active space orbitals in the complete active space computations, and natural charges. This material is available free of charge via the Internet at http://pubs.acs.org.

■ AUTHOR INFORMATION

Corresponding Author

*Fax: +91 222 576 7152. E-mail: sunoj@chem.iitb.ac.in.

Notes

The authors declare no competing financial interest.

■ ACKNOWLEDGMENTS

Generous computing time from IIT Bombay computer center is gratefully acknowledged. R.R. acknowledges CSIR (New Delhi) for a Senior Research Fellowship.

■ REFERENCES

(1) (a) Frimer, A. A. *Chem. Rev.* **1979**, *79*, 359. (b) Stratakis, M.; Orfanopoulos, M. *Tetrahedron* **2000**, *56*, 1595.

(2) (a) Sono, M.; Roach, M. P.; Coulter, E. D.; Dawson, J. H. *Chem. Rev.* **1996**, *96*, 2841. (b) Lara, M.; Mutti, F. G.; Glueck, S. M.; Kroutil, W. *J. Am. Chem. Soc.* **2009**, *131*, 5368. (c) Celaje, J. A.; Zhang, D.; Guerrero, A. M.; Selke, M. *Org. Lett.* **2011**, *13*, 4846. (d) Yin, H.; Xu, L.; Porter, N. A. *Chem. Rev.* **2011**, *111*, 5944 and references cited therein.

(3) (a) Shailaja, J.; Sivaguru, J.; Robbins, R. J.; Ramamurthy, V.; Sunoj, R. B.; Chandrasekhar, J. *Tetrahedron* **2000**, *56*, 6927. (b) Alberti, M. N.; Orfanopoulos, M. *Synlett.* **2010**, *7*, 999. (c) Saito, T.; Nishihara, S.; Kataoka, Y.; Nakanishi, Y.; Kitagawa, Y.; Kawakami, T.; Yamanaka, S.; Okumura, M.; Yamaguchi, K. *J. Phys. Chem. A* **2010**, *114*, 7967.

(4) (a) Vassilikogiannakis, G.; Margaros, I.; Montagnon, T. *Org. Lett.* **2004**, *6*, 2039. (b) Kao, T. C.; Chuang, G. J.; Liao, C. C. *Angew. Chem., Int. Ed.* **2008**, *47*, 7325.
(5) (a) Wasserman, H. H.; Gambale, R. J. *Tetrahedron* **1992**, *48*, 7059. (b) Wasserman, H. H.; Yoo, J. U.; DeSimone, R. W. *J. Am. Chem. Soc.* **1995**, *117*, 9772. (c) Wasserman, H. H.; Power, P.; Petersen, A. K. *Tetrahedron Lett.* **1996**, *37*, 6657. (d) Wasserman, H. H.; Xia, M.; Wang, J.; Petersen, A. K.; Jorgensen, M. *Tetrahedron Lett.* **1999**, *40*, 6145. (e) Wasserman, H. H.; Wiberg, K. B.; Larsen, D. L.; Parr, J. *J. Org. Chem.* **2005**, *70*, 105. (f) Alberti, M. N.; Vougioukalakis, G. C.; Orfanopoulos, M. *J. Org. Chem.* **2009**, *74*, 7274.
(6) (a) Adam, W.; Prein, M. *Acc. Chem. Res.* **1996**, *29*, 275. (b) Garavelli, M.; Bernardi, F.; Olivucci, M.; Robb, M. A. *J. Am. Chem. Soc.* **1998**, *120*, 10210. (c) Adam, W.; Saha-Mo1ller, C. R.; Schambony, S. B. *J. Am. Chem. Soc.* **1999**, *121*, 1834. (d) Bobrowski, M.; Liwo, A.; Ołdziej, S.; Jeziorek, D.; Ossowski, T. *J. Am. Chem. Soc.* **2000**, *122*, 8112. (e) Maranzana, A.; Ghigo, G.; Tonachini, G. *J. Am. Chem. Soc.* **2000**, *122*, 1414. (f) Sevin, F.; McKee, M. L. *J. Am. Chem. Soc.* **2001**, *123*, 4591. (g) Maranzana, A.; Ghigo, G.; Tonachini, G. *Chem.—Eur. J.* **2003**, *9*, 2616. (h) Singleton, D. A.; Hang, C.; Szymanski, M. J.; Meyer, M. P.; Leach, A. G.; Kuwata, K. T.; Chen, J. S.; Greer, A.; Foote, C. S.; Houk, K. N. *J. Am. Chem. Soc.* **2003**, *125*, 1319. (i) Yun, Li, Y.; Hu, H. Y.; Ye, J. P.; Fun, H. K.; Hu, H. W.; Xu, J. H. *J. Org. Chem.* **2004**, *69*, 2332. (j) Maranzana, A.; Canepa, C.; Ghigo, G.; Tonachini, G. *Eur. J. Org. Chem.* **2005**, 3643. (k) Leach, A. G.; Houk, K. N.; Foote, C. S. *J. Org. Chem.* **2008**, *73*, 8511. (l) Chung, L. W.; Li, X.; Sugimoto, H.; Shiro, Y.; Morokuma, K. *J. Am. Chem. Soc.* **2008**, *130*, 12299. (m) Alberti, M. N.; Vassilikogiannakis, G.; Orfanopoulos, M. *Org. Lett.* **2008**, *10*, 3997.
(7) (a) Wasserman, H. H.; Murray, R. W. *Singlet oxygen*; Academic Press: New York, 1979. (b) Stephenson, L. M.; Grdina, M. J.; Orfanopoulos, M. *Acc. Chem. Res.* **1980**, *13*, 419. (c) Orfanopoulos, M.; Stephenson, L. M. *J. Am. Chem. Soc.* **1980**, *102*, 1417. (d) Orfanopoulos, M.; Smonou, I.; Foote, C. S. *J. Am. Chem. Soc.* **1990**, *112*, 3607. (e) Orfanopoulos, M.; Stratakis, M.; Elemes, Y. *J. Am. Chem. Soc.* **1990**, *112*, 6417. (f) Stratakis, M.; Orfanopoulos, M; Foote, C. S. *Tetrahedron Lett.* **1991**, *32*, 863. (g) Orfanopoulos, M.; Stratakis, M. *Tetrahedron Lett.* **1991**, *32*, 7321. (h) Stratakis, M.; Orfanopoulos, M.; Foote, C. S. *J. Org. Chem.* **1998**, *63*, 1315. (i) Clennan, E. L. *Tetrahedron* **2000**, *56*, 9151. (j) Clennan, E. L.; Pace, A. *Tetrahedron* **2005**, *61*, 6665. (k) Alberti, M. N.; Orfanopoulos, M. *Chem.—Eur. J.* **2010**, *16*, 9414. (l) Also see ref 6.
(8) Harding, L. B.; Goddard, W. A. III. *J. Am. Chem. Soc.* **1977**, *99*, 4520.
(9) Bartlett, P. D.; Schaap, A. P. *J. Am. Chem. Soc.* **1970**, *92*, 3223.
(10) Kearns, D. R. *Chem. Rev.* **1971**, *71*, 395.
(11) (a) Mazur, S.; Foote, C. S. *J. Am. Chem. Soc.* **1970**, *92*, 3225. (b) Foote, C. S.; Dzakpasu, A. A.; Lin, J. H. P. *Tetrahedron Lett.* **1975**, *16*, 1247. (c) Eriksen, J.; Foote, C. S.; Parker, T. L. *J. Am. Chem. Soc.* **1977**, *99*, 6455.
(12) Foote, C. S.; Denny, R. W. *J. Am. Chem. Soc.* **1971**, *93*, 5162.
(13) Dewar, M. J. S.; Thiel, W. *J. Am. Chem. Soc.* **1975**, *97*, 3978.
(14) (a) Paquette, L. A.; Carr, R. V. C.; Arnold, E.; Clardy, J. *J. Org. Chem.* **1980**, *45*, 4907. (b) Adam, W.; Nestler, B. *J. Am. Chem. Soc.* **1993**, *115*, 5041. (c) Li, X.; Ramamurthy, V. *J. Am. Chem. Soc.* **1996**, *118*, 10666. (d) Vassilikogiannakis, G.; Stratakis, M.; Orfanopoulos, M.; Foote, C. S. *J. Org. Chem.* **1999**, *64*, 4130. (e) Kaanumalle, L. S.; Shailaja, J.; Robbins, R. J.; Ramamurthy, V. *J. Photochem. Photobiol. A* **2002**, *153*, 55. (f) Kannumalle, L. S.; Sivaguru, J.; Arunkumar, N.; Karthikeyan, S.; Ramamurthy, V. *Chem. Commun.* **2003**, 116. (g) Griesbeck, A. G.; El-Idreesy, T. T.; Lex, J. *Tetrahedron* **2006**, *62*, 10615. (h) Fudickar, W.; Vorndran, K. J.; Linker, T. *Tetrahedron* **2006**, *62*, 10639. (i) Stratakis, M.; Raptis, C.; Sofikiti, N.; Tsangarakis, C.; Kosmas, G.; Zaravinos, I. P.; Kalaitzakis, D.; Stavroulakis, D.; Baskakis, C.; Stathoulopoulou, A. *Tetrahedron* **2006**, *62*, 10623. (j) Sabbani, S.; Pensee, L. L.; Bacsa, J.; Hedenstrom, E.; O'Neill, P. M. *Tetrahedron* **2009**, *65*, 8531. (k) Sabbani, S.; La Pensee, L.; Bacsa, J.; Hedenstrom, E.; O'Neill, P. M. *Tetrahedron* **2009**, *65*, 8531.
(15) Sivaguru, J.; Solomon, M. R.; Poon, T.; Jockusch, S.; Bosio, S. G.; Adam, W.; Turro, N. J. *Acc. Chem. Res.* **2008**, *41*, 387.
(16) (a) Adam, W.; Bosio, S. G.; Turro, N. J. *J. Am. Chem. Soc.* **2002**, *124*, 8814. (b) Adam, W.; Bosio, S. G.; Turro, N. J. *J. Am. Chem. Soc.* **2002**, *124*, 14004. (c) Adam, W.; Bosio, S. G.; Turro, N. J. *J. Org. Chem.* **2004**, *69*, 1704. (d) Catak, S.; Celik, H.; Demir, A. S.; Aviyente, V. *J. Phys. Chem. A.* **2007**, *111*, 5855.
(17) (a) Janardanan, D.; Sunoj, R. B. *J. Org. Chem.* **2007**, *72*, 331. (b) Janardanan, D.; Sunoj, R. B. *Chem.—Eur. J.* **2007**, *13*, 4805. (c) Shinisha, C. B.; Sunoj, R. B. *Org. Bimol. Chem.* **2007**, *5*, 1287. (d) Janardanan, D; Sunoj, R. B. *J. Org. Chem.* **2008**, *73*, 8163. (e) Patil, M. P.; Sunoj, R. B. *Chem.—Eur. J.* **2008**, *14*, 10472. (f) Shinisha, C. B.; Sunoj, R. B. *Org. Bimol. Chem.* **2008**, *6*, 3921. (g) Sharma, A. K.; Sunoj, R. B. *Angew. Chem., Int. Ed.* **2010**, *49*, 6373. (h) Sharma, A. K.; Sunoj, R. B. *Chem. Commun.* **2011**, *47*, 5759. (i) Rajeev, R.; Sunoj, R. B. *Org. Bimol. Chem.* **2011**, *9*, 2123.
(18) (a) Shinisha, C. B.; Sunoj, R. B. *J. Am. Chem. Soc.* **2010**, *132*, 12319. (b) Shinisha, C. B.; Sunoj, R. B. *Org. Lett.* **2010**, *12*, 2868.
(19) Frisch, M. J. et al. *Gaussian 03*, Revision C.02; Gaussian, Inc.: Wallingford, CT, 2004. A complete reference is provided in the Supporting Information.
(20) (a) Reed, A. E.; Curtiss, L. A.; Weinhold, F. *Chem. Rev.* **1988**, *88*, 899. (b) Glendening, E. D.; Reed, A. E.; Carpenter, J. E.; Weinhold, F. NBO Version 3.1. (c) Frisch, M. J. et al. *Gaussian 09*, Revision A.02; Gaussian, Inc.: Wallingford, CT, 2004. A complete reference is provided in the Supporting Information.
(21) (a) Becke, A. D. *Phys. Rev. A* **1988**, *38*, 3098. (b) Lee, C.; Yang, W.; Parr, R. G. *Phys. Rev. B* **1988**, *37*, 785. (c) Becke, A. D. *J. Chem. Phys.* **1993**, *98*, 5648.
(22) (a) Noodleman, L. *J. Chem. Phys.* **1981**, *74*, 5737. (b) Noodleman, L.; Davidson, E. R. *Chem. Phys.* **1986**, *109*, 131. (c) Noodleman, L.; Case, D. A.; Aizman, A. *J. Am. Chem. Soc.* **1988**, *110*, 1001.
(23) (a) Yamaguchi, K.; Jensen, F.; Dorigo, A.; Houk, K. N. *Chem. Phys. Lett.* **1988**, *149*, 537. (b) Yamanaka, S.; Kawakami, T.; Nagao, H.; Yamaguchi, K. *Chem. Phys. Lett.* **1994**, *231*, 25. (c) Values are also calculated with the method proposed in: Wittbrodt, J. M.; Schlegel, H. B. *J. Chem. Phys.* **1996**, *105*, 6574. No significant deviations were noticed between both these methods.
(24) (a) Gonzalez, C.; Schlegel, H. B. *J. Chem. Phys.* **1989**, *90*, 2154. (b) Gonzalez, C.; Schlegel, H. B. *J. Phys. Chem.* **1990**, *94*, 5523.
(25) Inclusion of molecular orbitals, which are directly taking part in the reaction, is based on the previous suggestion as reported in ref 6k.
(26) Detailed description and qualitative figures of molecular orbitals is given in the Supporting Information. See Figures S1−S3.
(27) Attempts to include MP2 corrections on CAS(12,10) energies yielded only CASSCF energies. More importantly, exclusion of MP2 corrections from the CAS computations led to results, which did not agree with the experimentally reported stereochemical outcome.
(28) (a) Roos, B. O.; Szulkin, M.; Jaszufiski, M. *Theor. Chim. Acta* **1987**, *71*, 375. (b) Yoshioka, Y.; Tsunesada, T.; Yamaguchi, K.; Saito, I. *Int. J. Quantum Chem.* **1997**, *65*, 787. (c) Hoffner, J.; Schottelius, M. J.; Feichtinger, D.; Chen, P. *J. Am. Chem. Soc.* **1998**, *120*, 376. (d) Mousavipour, S. H.; Homayoon, Z. *J. Phys. Chem. A* **2003**, *107*, 8566. (e) Guo, Y.; Bhattacharya, A.; Bernstein, E. R. *J. Chem. Phys.* **2011**, *134*, 24318. (f) Also see ref 6k.
(29) One of the earliest suggestions was due to Fukui et al. who proposed that four key approaches are important in singlet oxygenation reaction of olefins. See: Inagaki, S.; Fukui, K. *J. Am. Chem. Soc.* **1975**, *97*, 7480.
(30) Energies of subsequent transition structures from this conformer are also found to be consistently higher. These results are summarized in Table S1 in the Supporting Information.
(31) Results of DFT(RB3LYP) and DFT(UB3LYP) calculations are summarized in Figures S4 and S5 in the Supporting Information. Calculations at the RB3LYP level of theory reproduce experimental results, while UB3LYP failed to do so.
(32) Natural charges on nitrogen and oxygen are respectively found to be −0.41 and −0.38 by NBO analysis.

(33) The O1−O2 distance in free singlet oxygen is 1.21 Å and the degree of pyramidalization around C2 of the free enecarbamate is found to be as little as 0.02° at the same level of theory.
(34) Complete details of the charge analysis are provided in Table S2 in the Supporting Information.
(35) The natural charge on the nitrogen atom is found to decrease from −0.52 in *E*-enecarbamate to −0.45 in IM1-syn. Details are given in Table S2 in the Supporting Information.
(36) Reported stereoselectivity for the [2 + 2] mode of addition in a similar substrate (with C-4 isopropyl oxazolidinone) is >99. The *Z*-isomers of enecarbamates in general give selectivities above 98%. (ref 15).
(37) The dihedral angles that molecular oxygen makes with enecarbamate (C1−C2−O2−O1) are respectively 58.83° and −61.82° in TS2-syn and TS5-syn.
(38) (a) Diefenbach, A.; Bickelhaupt, F. M. *J. Phys. Chem. A* **2004**, *108*, 8460. (b) Jong, G. T. D.; Visser, R.; Bickelhaupt, F. M. *J. Organomet. Chem.* **2006**, *691*, 4341. (c) Jong, G. T. D.; Bickelhaupt, F. M. *Chem. Phys. Chem* **2007**, *8*, 1170. (d) Jong, G. T. D.; Bickelhaupt, F. M. *J. Chem. Theory Comput.* **2007**, *3*, 514. (e) Fernández, I.; Bickelhaupt, F. M.; Cossío, F. P. *Chem.—Eur. J.* **2009**, *15*, 13022.
(39) The dihedral angle between the molecular oxygen and unsaturated bond in enecarbamate as given by C1-C2-O2-O1 is 16.05°.
(40) Extended IRC calculations indicated the lack of existence of any intermediate. See Figure S8 in Supporting Information.
(41) Sheppard, A. N.; Acevedo, O. *J. Am. Chem. Soc.* **2009**, *131*, 2530.
(42) Experimentally reported de for the reaction is 88:12 (ref 15).
(43) Relative free energies of PD2 and PD4 are respectively found to be −112.2 and −94.6 kcal mol^{-1} with reference to separated reactants (singlet oxygen and *E*- enecarbamate).
(44) Results of RB3LYP and UB3LYP calculations are summarized in Figures S6 and S7 in Supporting Information. Similar to *E*-isomer, calculations at the DFT(RB3LYP) level of theory reproduces experimental reports while DFT(UB3LYP) results were at variance with the experimental reports.
(45) Extended IRC calculations indicated the lack of existence of any intermediate. See Figure S8 in the Supporting Information
(46) IRC plots of transition structures are provided in Figure S8 in the Supporting Information. Relative free energies of PD6 and PD8 are respectively found to be −52.8 and −48.6 kcal mol^{-1} with reference to the separated reactants (singlet oxygen and *Z*-enecarbamate).